

Provided for non-commercial research and education use.
Not for reproduction, distribution or commercial use.



This article appeared in a journal published by Elsevier. The attached copy is furnished to the author for internal non-commercial research and education use, including for instruction at the authors institution and sharing with colleagues.

Other uses, including reproduction and distribution, or selling or licensing copies, or posting to personal, institutional or third party websites are prohibited.

In most cases authors are permitted to post their version of the article (e.g. in Word or Tex form) to their personal website or institutional repository. Authors requiring further information regarding Elsevier's archiving and manuscript policies are encouraged to visit:

<http://www.elsevier.com/authorsrights>



Contents lists available at ScienceDirect

Electrochimica Acta

journal homepage: www.elsevier.com/locate/electacta

Scaling laws for carbon-based electric double layer capacitors



Hainan Wang, Jin Fang, Laurent Pilon*

University of California, Los Angeles, Henry Samueli School of Engineering and Applied Science, Mechanical and Aerospace Engineering Department, 420 Westwood Plaza, Los Angeles, CA 90095, USA

ARTICLE INFO

Article history:

Received 31 May 2013

Received in revised form 5 July 2013

Accepted 6 July 2013

Available online 19 July 2013

Keywords:

Mesoporous carbon

Supercapacitors

Modeling

Similarity

Modified Poisson–Boltzmann model

ABSTRACT

This paper presents scaling laws for the integral capacitance of electric double layer capacitors (EDLCs) supported by rigorous analysis and experimental data for porous carbon-based electrodes. First, dimensionless similarity parameters were identified based on dimensional analysis of the modified Poisson–Boltzmann model for binary and symmetric electrolytes. Then, a correlation for the equilibrium potential at the Stern/diffuse layer interface near planar electrodes and near cylindrical and spherical pores was obtained as a function of previously identified dimensionless numbers for a wide range of parameters. Similarly, an analytical expression was proposed for the dimensionless double layer integral capacitance of planar electrodes. Finally, scaling analysis was applied to experimentally measured integral capacitance of mesoporous carbon electrodes with a wide range of morphology and different electrolytes. To maximize the integral areal capacitance, the electrolyte should have small ion effective diameter and large dielectric constant. The electrode pore diameter should be tailored to match the ion diameter.

© 2013 Elsevier Ltd. All rights reserved.

1. Introduction

Electric double layer capacitors (EDLCs) have been the subject of intense studies in recent years due to their promise as electrical energy storage devices in high power applications [1–4]. EDLCs store electric charges physically in the electric double layer (EDL) forming at electrode/electrolyte interfaces. Fig. 1a and b shows schematics of the electric double layer structure forming near a positively charged surface of a planar electrode and of a cylindrical or spherical pores, respectively. Solvated anions of effective diameter a migrate and adsorb at the electrode surface due to electrostatic forces while the solvated cations are repelled [5]. The Stern layer is defined as the compact layer near the electrode surface [5]. Note that there are no free charges within the Stern layer [5]. Beyond the Stern layer is the so-called diffuse layer where ions are mobile under the coupled influence of electrostatic forces and diffusion [5].

Electrodes of EDLCs are typically made of porous carbon-based materials [1–3]. The porous structure increases the electrode surface area per unit volume available for EDL formation thus increasing energy density. However, the relationship between energy density and surface area is neither linear nor straightforward. The capacitance of EDLCs depends on a variety of parameters such as the electrode surface area, pore size, electrolyte properties, and the potential window [1–3]. General correlations relating the

capacitance of EDLCs to the physical or electrochemical properties of the electrodes and electrolytes and accounting for the detailed structure of the electric double layer are not available. Instead, progress has been made mainly by trial and error informed by physical intuition and simplified EDLC models [6–9].

This study aims to develop an experimentally validated correlation relating the integral areal capacitance of EDLCs to these parameters. Such correlations would rationalize the design of EDLCs and provide rules for optimizing the porous architecture of EDLCs and for selecting the electrolyte.

2. Background

2.1. Equilibrium model – planar electrode

The modified Poisson–Boltzmann (MPB) model for binary and symmetric electrolytes predicts the equilibrium electric potential ψ in the electrolyte and accounts for the finite ion size [10,11]. In one-dimensional Cartesian coordinates corresponding to a planar electrode, it is expressed as [10]

$$\frac{\partial}{\partial x} \left(\epsilon_0 \epsilon_r \frac{\partial \psi}{\partial x} \right) = \frac{2zeN_A c_\infty \sinh((ze\psi)/(k_B T))}{1 + 4N_A a^3 c_\infty \sinh^2((ze\psi)/(2k_B T))} \quad (1)$$

where ϵ_0 and ϵ_r are the free space permittivity ($\epsilon_0 = 8.854 \times 10^{-12}$ F/m) and the relative permittivity of the electrolyte solution, respectively. The Boltzmann constant is denoted by $k_B = 1.38 \times 10^{-23}$ J/K while T is the absolute temperature, z is the ion valency, $e = 1.602 \times 10^{-19}$ C is the elementary

* Corresponding author. Tel.: +1 310 206 5598; fax: +1 310 206 2302.
E-mail address: pilon@seas.ucla.edu (L. Pilon).

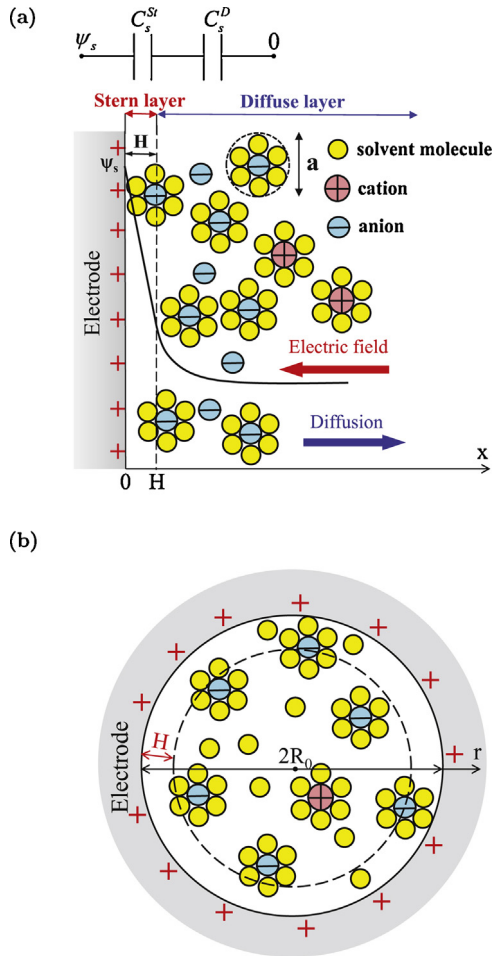


Fig. 1. A schematic of the electric double layer structure showing solvated anions and cations arrangement near the surface of (a) a planar electrode and (b) a cylindrical or spherical pore.

charge, and $N_A = 6.022 \times 10^{23} \text{ mol}^{-1}$ is the Avogadro constant. The effect of the Stern layer can be accounted for via a boundary condition at the Stern/diffuse layer interface located at $x=H$ expressed as [12,13]

$$-\frac{\partial \psi}{\partial x}(x=H) = \frac{\psi_s - \psi_D}{H} \quad (2)$$

where ψ_s is the surface potential and H is the Stern layer thickness corresponding to half of the effective ion diameter a , i.e., $H=a/2$, as illustrated in Fig. 1. The potential at the Stern layer/diffuse layer interface located at $x=H$ is denoted by $\psi_D = \psi(H)$. The electric potential far away from the electrode was imposed as zero, i.e., $\psi(x=L) = 0$. Note that this boundary condition is valid for symmetric electrolytes but cannot be used for asymmetric electrolytes [14].

Solving Eqs. (1) and (2) yields expression for the equilibrium Stern and diffuse layer capacitances for planar electrodes in binary and symmetric electrolytes, denoted by C_s^{St} and C_s^D , respectively. Assuming constant electrolyte properties and accounting for the finite ion size, they are expressed as [10,15–17]

$$C_s^{St} = \frac{\epsilon_0 \epsilon_r}{H} \quad \text{and} \quad C_s^D = \frac{2zeN_A c_\infty \lambda_D}{\psi_D} \sqrt{\frac{2}{v_p} \ln \left[1 + 2v_p \sinh^2 \left(\frac{ze\psi_D}{2k_B T} \right) \right]} \quad (3)$$

where λ_D is the Debye length for symmetric electrolytes defined as $\lambda_D = \sqrt{\epsilon_0 \epsilon_r k_B T / 2e^2 z^2 N_A c_\infty}$ and corresponding to an estimate of the EDL thickness [5,18]. The packing parameter v_p is defined as $v_p = 2a^3 N_A c_\infty$. It represents the ratio of the total bulk ion concentration to the maximum ion concentration assuming a simple cubic ion packing [10,15–17]. By treating the Stern and diffuse layer capacitances in series, the total double layer integral areal capacitance $C_{s,planar}$ can be expressed as [5,19,16,20,17]

$$\frac{1}{C_{s,planar}} = \frac{1}{C_s^{St}} + \frac{1}{C_s^D} = \frac{a}{2\epsilon_0 \epsilon_r} + \frac{\psi_D}{2zeN_A c_\infty \lambda_D} \left\{ \frac{2}{v_p} \ln \left[1 + 2v_p \sinh^2 \left(\frac{ze\psi_D}{2k_B T} \right) \right] \right\}^{-1/2} \quad (4)$$

2.2. Cylindrical and spherical pores

The MPB model with Stern layer for cylindrical or spherical pores is expressed as [16,17]

$$\frac{1}{r^p} \frac{\partial}{\partial r} \left(\epsilon_0 \epsilon_r r^p \frac{\partial \psi}{\partial r} \right) = zeN_A c_\infty \frac{2 \sinh((ze\psi)/(k_B T))}{1 + 4N_A a^3 c_\infty \sinh^2((ze\psi)/(2k_B T))} \quad (5)$$

where $p=1$ or 2 for cylindrical or spherical pores, respectively. Here also, the effect of the Stern layer can be accounted for via the boundary condition at the Stern/diffuse layer interface, located at $r=R_0 - H$, expressed as [17]

$$\frac{\partial \psi}{\partial r}(r=R_0 - H) = \begin{cases} \frac{\psi_s - \psi_D}{(R_0 - H) \ln(R_0/(R_0 - H))} & \text{for cylindrical pores} \quad (6a) \\ \frac{\psi_s - \psi_D}{H} \frac{R_0}{R_0 - H} & \text{for spherical pores} \quad (6b) \end{cases} \quad (6)$$

where ψ_D is the potential at the Stern layer/diffuse layer interface, i.e., $\psi_D = \psi(r=R_0 - H)$. Moreover, the gradient of electric potential at the center of the spherical or cylindrical pore (at $r=0$) was imposed as zero by virtue of symmetry, i.e.,

$$\frac{\partial \psi}{\partial r}(r=0) = 0 \quad (7)$$

To the best of our knowledge, unlike for planar electrodes, no analytical expressions exist for the total and diffuse layer capacitances of cylindrical or spherical pores when accounting for the finite ion size.

This paper aims to identify scaling laws governing the integral areal capacitance of actual EDLCs with porous carbon-based electrodes as a function of the dimensionless similarity parameters rigorously identified from scaling analysis of the governing equations for the electric potential and ion concentrations.

3. Analysis

3.1. Equilibrium modified Poisson–Boltzmann model

3.1.1. Planar electrodes

The dimensional analysis of the MPB model can be performed by scaling (i) the spatial coordinate by the Debye length λ_D and (ii) the local potential ψ by the thermal voltage $k_B T/ez$ representing the voltage that would induce a potential energy equivalent to the thermal energy of an ion of charge z so that [21]

$$x^* = \frac{x}{\lambda_D} \quad \text{and} \quad \psi^* = \frac{\psi}{k_B T/ez} \quad (8)$$

Then, Eq. (1) can be written in dimensionless form as

$$\frac{\partial^2 \psi^*}{\partial x^{*2}} = \frac{2 \sinh \psi^*}{1 + 2\nu_p \sinh^2(\psi^*/2)}. \quad (9)$$

Moreover, the dimensionless boundary conditions can be written as

$$-\frac{\partial \psi^*}{\partial x^*} \left(x^* = \frac{a^*}{2} \right) = \frac{\psi_s^* - \psi_D^*}{a^*/2} \quad \text{and} \quad \psi^*(x^* = L^*) = 0. \quad (10)$$

where $\psi_D^* = \psi_D/(k_B T/ez) = \psi^*(a^*/2)$ is the dimensionless diffuse layer potential. Four dimensionless similarity parameters arise from the scaling analysis of the equilibrium MPB model with Stern layer for planar electrodes (Eqs. (9) and (10)) namely (i) the dimensionless surface potential $\psi_s^* = \psi_s/(k_B T/ze)$, (ii) the packing parameter $\nu_p = 2N_A a^3 c_\infty$, (iii) the dimensionless ion diameter $a^* = a/\lambda_D = 2H/\lambda_D$, and (iv) the dimensionless electrolyte layer thickness $L^* = L/\lambda_D$. Note that these four dimensionless numbers, or combination thereof, were also derived from scaling analysis of the modified Poisson–Nernst–Planck (MPNP) model [20]. In the scaling analysis of the MPNP model, an additional number was obtained corresponding to the dimensionless scan rate. The two approaches are equivalent if one considers low scan rates and imposes $\psi_s = \Delta\psi/2$ where $\Delta\psi$ is the potential window used in cyclic voltammetry simulations [20].

Similarly, scaling the total integral areal capacitance of a planar electrode $C_{s,planar}$ (Eq. (3)) by the Stern layer capacitance $C_s^{St} = \epsilon_0 \epsilon_r / H$ with $H = a/2$, results in the dimensionless total integral areal capacitance $C_{s,planar}^*$ expressed as,

$$\frac{1}{C_{s,planar}^*} = \frac{C_s^{St}}{C_{s,planar}} = 1 + \frac{2\psi_D^*}{a^*} \left\{ \frac{2}{\nu_p} \ln \left[1 + 2\nu_p \sinh^2 \left(\frac{\psi_D^*}{2} \right) \right] \right\}^{-1/2} \quad (11)$$

To the best of our knowledge, analytical expressions for the diffuse layer potentials ψ_D or ψ_D^* do not exist when accounting for the finite ion size, i.e., when $\nu_p \neq 0$. Alternatively, they can be determined numerically by solving the equilibrium modified Poisson–Boltzmann (MPB) model with the Stern layer (Eqs. (1) and (2)). If the above scaling analysis is correct, ψ_D^* should depend only on the four dimensionless numbers identified namely ν_p , a^* , L^* , and ψ_s^* .

3.1.2. Cylindrical and spherical pores

By employing the scaling parameters $r^* = r/\lambda_D$ and $\psi^* = \psi/(k_B T/ez)$, the MPB model with Stern layer (Eq. (5)–(7)) for cylindrical and spherical pores can be written in dimensionless form as

$$\frac{1}{r^{*p}} \frac{\partial}{\partial r^*} \left(r^{*p} \frac{\partial \psi^*}{\partial r^*} \right) = \frac{2 \sinh \psi^*}{1 + 2\nu_p \sinh^2(\psi^*/2)} \quad (12)$$

The dimensionless boundary conditions at the Stern/diffuse layer interface can be written as,

$$\frac{\partial \psi^*}{\partial r^*} \left(r^* = R_0^* - \frac{a^*}{2} \right) = \begin{cases} \frac{\psi_s^* - \psi_D^*}{(R_0^* - a^*/2) \ln((R_0^*/(R_0^* - a^*/2)))} & \text{for cylindrical pores} \\ \frac{\psi_s^* - \psi_D^*}{a^*/2} \frac{R_0^*}{R_0^* - a^*/2} & \text{for spherical pores} \end{cases} \quad (13)$$

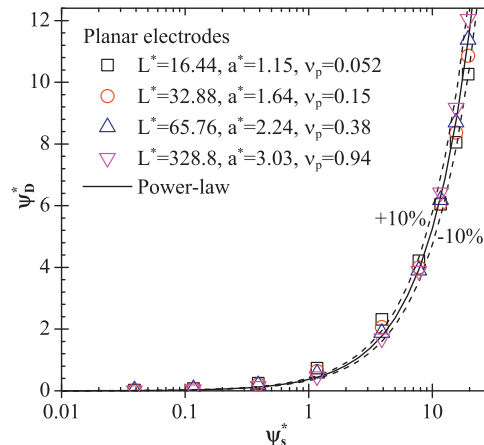


Fig. 2. Dimensionless diffuse layer potential ψ_D^* as a function of dimensionless surface potential ψ_s^* ranging from 0.01 to 20 for different values of L^* , a^* , and ν_p .

where $\psi_D^* = \psi^*(R_0^* - a^*/2)$. The symmetry boundary condition at the center of the pore is given by,

$$\frac{\partial \psi^*}{\partial r^*} (r^* = 0) = 0. \quad (14)$$

Here also, four dimensionless numbers appeared in the dimensionless MPB model with Stern layer (Eqs. (12)–(14)) for cylindrical and spherical pores, namely (i) ψ_s^* , (ii) ν_p , (iii) a^* , and (iv) the dimensionless pore radius defined as $R_0^* = R_0/\lambda_D$. The only difference from the dimensionless numbers governing the integral areal capacitance of planar electrodes is the substitution of L^* by R_0^* .

4. Results and discussion

4.1. Equilibrium diffuse layer potential

4.1.1. Planar electrodes

Fig. 2 shows the dimensionless diffuse layer potential ψ_D^* as a function of the dimensionless surface potential window ψ_s^* ranging from 0.01 to 20 with L^* varying between 16 and 329, while ν_p ranged from 0.052 to 0.94, and a^* from 1.15 to 3.03. It was computed by numerically solving the equilibrium MPB model with the Stern layer (Eqs. (9) and (10)). It is evident that all data points nearly collapsed on a single line irrespective of the values of ν_p , a^* , and L^* so that ψ_D^* depended solely on ψ_s^* . The inter-electrode distance $2L$ did not affect ψ_D provided that the electric double layer on each electrode did not overlap the other, i.e., for $L \gg \lambda_D$ or $L^* \gg 1$. Then, the dimensionless diffuse layer potential ψ_D^* as a function of ψ_s^* was fitted with a power law to yield

$$\psi_D^* = 0.37 \psi_s^{*1.16} \quad (15)$$

The associated coefficient of determination was $R^2 = 0.98$. Predictions of C_s^D using Eq. (3) and the above expression for ψ_D^* fell within 1% of its value obtained using the numerically computed value of ψ_D .

4.1.2. Cylindrical and spherical pores

Fig. 3 shows the predicted dimensionless diffuse layer potential ψ_D^* as a function of dimensionless surface potential window ψ_s^* ranging from 0.01 to 20 for (a) cylindrical and (b) spherical pores with dimensionless pore radius $R_0^* = 6.58, 11.5, 16.44, 65.76, \text{ and } 328.8$. These values correspond to surface potential ψ_s ranging from 0.001 to 0.5 V and R_0 equals to 2, 3.5, 5, 20, and 100 nm, respectively. Here, ν_p ranged from 0.15 to 0.94 and a^* from 1.64 to 3.03. The dimensionless diffuse layer potential ψ_D^* for planar electrodes given by Eq. (15) was also shown in Fig. 3 for comparison. It is evident that

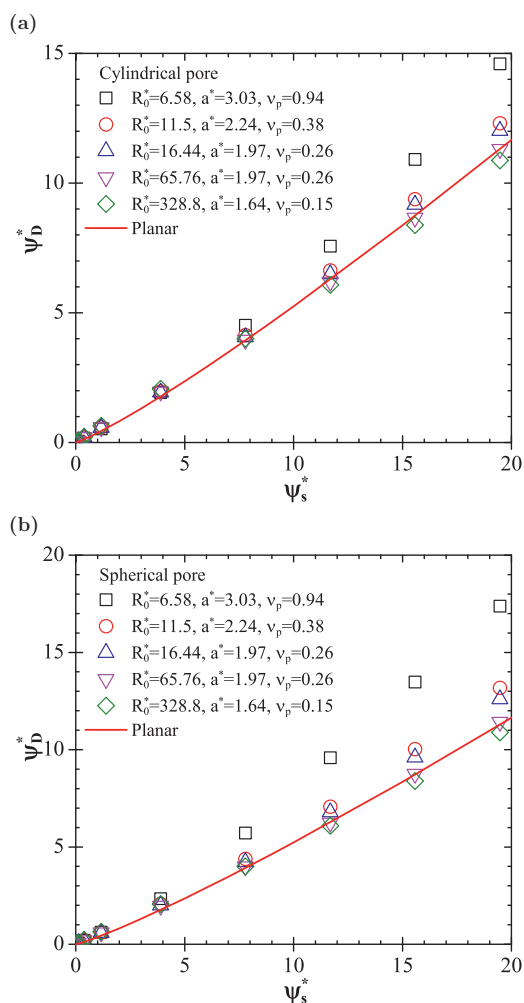


Fig. 3. Predicted dimensionless diffuse layer potential ψ_D^* as a function of dimensionless surface potential ψ_s^* for (a) cylindrical and (b) spherical pores obtained from MPB model with Stern layer for different values of R_0^* , a^* , and v_p .

ψ_D^* for cylindrical or spherical pores was nearly identical to that of planar electrodes for $R_0^* \geq 16$. For $R_0^* < 16$, the predicted ψ_D^* for cylindrical or spherical pores was larger than that of planar electrodes. The difference increased with increasing ψ_s^* and decreasing R_0^* . The

maximum difference was less than 15% and 30% for cylindrical and spherical pores, respectively, for the range of R_0^* and ψ_s^* considered. Overall, these results demonstrate that the correlation for the equilibrium diffuse layer potential for planar electrodes (Eq. (15)) may be applied to cylindrical or spherical pores with acceptable accuracy.

4.2. Equilibrium integral areal capacitance

Combining Eqs. (11) and (15), the dimensionless equilibrium integral areal capacitance $C_{s,planar}^*$ for planar electrodes can be expressed in terms of the three dimensionless numbers identified previously ψ_s^* , v_p , and a^* as

$$\frac{1}{C_{s,planar}^*} = 1 + \frac{0.74\psi_s^{*1.16}}{a^*} \left\{ \frac{2}{v_p} \ln [1 + 2v_p \sinh^2(0.185\psi_s^{*1.16})] \right\}^{-1/2} \quad (16)$$

Note that, under equilibrium conditions, $C_{s,planar}^*$ does not depend on L^* as also observed in CV simulations at low scan rates [20]. This analytical expression enables the prediction of the integral areal capacitance of planar electrodes without solving the MPB model.

4.3. Experimental data

A wide range of experimental data was collected from the literature in order to assess the applicability of the above scaling analysis to actual carbon-based porous electrodes. Experimental data were selected to ensure that (i) the electrolytes were binary and symmetric such as KOH and TEABF₄, (ii) the reported capacitance was the integral areal capacitance and not the differential areal capacitance, and (iii) the integral areal capacitance was measured using either cyclic voltammetry at low scan rates or galvanostatic charge/discharge at low currents corresponding to the quasi-equilibrium regime. Then, the integral areal capacitances measured by two techniques were identical as quasi-equilibrium conditions prevailed [20,22]. It is convenient to consider the areal capacitance as it accounts for the possibility that electrodes might have different porosity and surface area per unit volume.

Table 1 summarizes the experimental data reported in the literature for EDLCs with various electrolytes, electrode pore radii R_0 , and potential windows $\Delta\psi = 2\psi_s$ along with the corresponding range of the experimentally measured integral areal capacitance,

Table 1

Summary of experimental data reported in the literature for various carbon electrodes, binary and symmetric electrolytes, potential window $\Delta\psi = 2\psi_s$, and average pore radius R_0 along with their integral areal capacitance $C_{s,exp}$ (in $\mu\text{F}/\text{cm}^2$).

Ref.	Electrode	R_0 (nm)	Electrolyte	$\Delta\psi = 2\psi_s$ (V)	$C_{s,exp}$ ($\mu\text{F}/\text{cm}^2$)
[23]	TiC-CDC	0.68–1.09	1 M TEABF ₄ in AN	2.3	6.0–13.6
[24]	OMC-M	2.15–4.25	6.88 M KOH	0.8	16.8–27.5
[24]	OMC-K	1.95–4.7	6.88 M KOH	0.8	12.0–22.5
[30]	GNS/CB	0.364–0.37	6 M KOH	1	28.3–46.6
[29]	HOMC	0.37–0.41	6 M KOH	1	8.2–11.2
[31]	FSMC	2.15	6 M KOH	0.6	19.4
[25]	OMC	1.35–3.0	6 M KOH	1	5.8–11.8
[25]	OMC	1.35–3.0	1 M TEABF ₄ in AN	2	5.2–6.7
[26]	OMC	2.7–3.25	6.88 M KOH	0.89	11.9–15.0
[32]	CMK-8	2.39	2 M KOH	1	13.3
[32]	H-CMK-8	2.33	2 M KOH	1	20.2
[27]	OMC	2.25	6 M KOH	0.8	18.8
[38]	MC spheres	1.34	2 M KOH	1	11.1
[39]	MC	0.625–0.69	1 M TEABF ₄ in AN	2	10.3–11.6
[28]	OMC	0.395–0.555	1 M TEABF ₄ in PC	2	5.5–6.7
[33]	Carbon foam	1.9	6 M KOH	1	12.5
[40]	OMC	0.6	6 M KOH	0.8	14.1–19.6
[34]	GAC	0.245–0.26	6 M KOH	1	13.4–17.7
[35]	C-CS	1.95	6 M KOH	0.9	10.6–16

Note: Solvent for KOH was water.

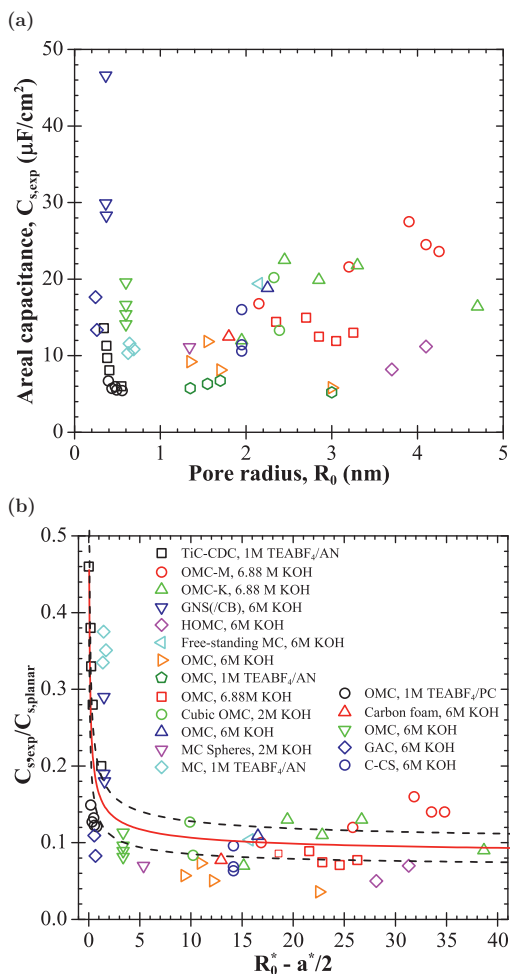


Fig. 4. (a) Experimental data of integral capacitance $C_{s,exp}$ as a function of pore radius R_0 and (b) the ratio $C_{s,exp}/C_{s,planar}$ as a function of $R_0^* - a^*/2$ for EDLCs with various mesoporous carbon electrodes and binary symmetric electrolytes.

denoted by $C_{s,exp}$ (in $\mu\text{F}/\text{cm}^2$). The electrodes consisted of various mesoporous carbons, namely (i) titanium carbide-derived carbon (TiC-CDC) [23], (ii) ordered mesoporous carbon (OMC) [24–28], (iii) highly ordered mesoporous carbon (HOMC) [29], (iv) graphene nanosheet (GNS) and graphene nanosheet/carbon black composites (GNS/CB) [30], (v) free-standing mesoporous carbon thin films (FSMC) [31], (vi) cubic mesoporous carbon (CMK), (vii) acid-modified CMK (H-CMK) [32], (viii) carbon foams [33], (ix) ginkgo activated carbon shells (GAC) [34], and (x) hierarchical porous core-shell carbon structure (C-CS) [35]. The electrode average pore radius varied from 0.36 to 3.25 nm. Three different electrolytes were considered including aqueous KOH and TEABF₄ in propylene carbonate (PC) or acetonitrile (AN) at concentrations c_∞ between 1 and 6.88 M. Anion and cation effective diameters typically differ, at least slightly. For example, OH⁻ and TEA⁺ ions are slightly larger than K⁺ and BF₄⁻, respectively. However, they were assumed to be identical. The non-solvated effective ion diameter a was taken as 0.35 nm for ions K⁺ and OH⁻ in water. It was assumed to be 0.68 nm for TEA⁺ and BF₄⁻ [36,23]. The potential window varied between 0.6 and 2.3 V depending on the electrolyte. Overall, a total of 56 experimental data points were collected corresponding to dimensionless numbers in the ranges $23 \leq \Delta\psi^* = 2\psi_s^* \leq 90$, $0.1 \leq \nu_p \leq 0.57$, $1.6 \leq a^* \leq 4.05$ (based on non-solvated ion diameters), and $1.4 \leq R_0^* \leq 40.2$.

Fig. 4a shows the reported integral areal capacitance $C_{s,exp}$ as a function of the reported average pore radius R_0 for the

above-mentioned experimental data. As expected, these data are scattered and the capacitance varies from 5.5 to 47 $\mu\text{F}/\text{cm}^2$ due to the wide range of electrolytes, electrode morphologies and pore sizes, and potential windows considered. On the other hand, Fig. 4b shows the same data plotted in terms of the ratio $C_{s,exp}/C_{s,planar}$ as a function of $R_0^* - a^*/2$ where $C_{s,planar} = 2\epsilon_0\epsilon_r C_{s,planar}^*/a$ was predicted using Eq. (16). It indicates that $C_{s,exp}/C_{s,planar}$ decreased from 0.5 to about 0.1 when $R_0^* - a^*/2$ increased from 0 to 40. First, it is remarkable that the experimental capacitances of mesoporous carbon electrodes had the same order of magnitude as the theoretical capacitance for planar electrodes $C_{s,planar}$. It is also worth noting that plotting the data in terms of $C_{s,exp}/C_{s,planar}$ versus $R_0^* - a^*/2$ significantly reduced the scatter compared to Fig. 4a and described a consistent trend. The capacitance ratio $C_{s,exp}/C_{s,planar}$ increased as the dimensionless pore radius R_0^* decreased and approached the dimensionless ion radius $a^*/2$. As the pore radius increased, the capacitance ratio $C_{s,exp}/C_{s,planar}$ reached a plateau of around 0.08. Curve fitting of the experimental data led to the following correlation,

$$\frac{C_{s,pred}}{C_{s,planar}} = 0.08 + \frac{0.084}{\sqrt{R_0^* - a^*/2}} \quad (17)$$

Fig. 4b also shows curves with $\pm 20\%$ deviations. The scatter in the experimental data and the fact that $C_{s,exp}$ differs from $C_{s,planar}$ for large values of R_0 can be attributed to the following main reasons: (i) experimentally, the pores featured a nonuniform size distribution while the scaling analysis was based on the reported average pore radius, (ii) the relative permittivity ϵ_r was assumed to be constant although it may vary significantly under high electric fields such as those encountered near the electrode surface [37,16], (iii) the electrolytes were assumed to be symmetric while anions and cations may have different solvated and/or non-solvated ion diameters, and (iv) the simple cubic packing of ions near the electrode assumed in formulating the MPB model may be overly simplistic. Note that attempts to account for the field-dependent dielectric constant in the Stern layer did not yield a better correlation (not shown). In other words, the semi-empirical constants in Eq. (17) overall accounted for this effect.

The scaling law given by Eq. (17) indicates that the equilibrium integral areal capacitance of mesoporous carbons with binary and symmetric electrolytes can be expressed as

$$C_{s,pred} = f\left(\frac{R_0^* - a^*}{2}\right) C_{s,planar} \quad (18)$$

where $C_{s,planar}$ is the equilibrium areal capacitance of the planar electrode given by Eq. (4) while $f(R_0^* - a^*/2)$ is a geometric function correcting for the fact that pore/electrolyte interfaces are not planar. It is constant in the limiting case when $R_0 \gg a/2$ or $R_0^* - a^*/2 \gg 1$ such that the effect of the pore curvature on the areal capacitance is negligible.

Sensitivity analysis of this semi-empirical model was performed by randomly sampling it with 1300 sets of input parameters with realistic electrolyte properties (i) a ranging from 0.1 to 1 nm, (ii) ϵ_r between 20 and 100, (iii) c_∞ from 1 to 6 M, and (iv) z with integer values between 1 and 3. The electrode properties were such that (v) R_0 ranged from 1 to 10 nm and (iv) ψ_s varied between 1 and 3 V. Scatter plots of $C_{s,pred}$ against each individual input variable indicate that the integral areal capacitance was most sensitive to the effective ion diameter a and to the electrolyte dielectric constant ϵ_r . This can be attributed to the fact that under large ion concentrations and potential windows, the total capacitance was dominated by the Stern layer capacitance expressed as $C_s^{st} = 2\epsilon_0\epsilon_r/a$ [16]. Interestingly, $C_{s,pred}$ was only weakly sensitive to the surface potential ψ_s . However, the fact that the total energy stored E (in J) is proportional to ψ_s^2 , i.e., $E = C\psi_s^2/2$ confirms the importance of maximizing the

surface potential or potential window to maximize EDLCs' performance. Similarly, $C_{s,pred}$ was weakly sensitive to the pore radius R_0 except for R_0 approaching a , as suggested by Eq. (17). Note that reducing the pore size also increases the interfacial area A_i between the electrode and the electrolyte and thus the total energy stored E and the capacitance C (in F) given by $C = C_{s,pred} \times A_i$.

5. Conclusion

This study presented scaling analysis of equilibrium model for the electric double layer integral areal capacitance $C_{s,planar}$ for planar electrodes in binary and symmetric electrolytes. It was based on a power law correlation for the equilibrium diffuse layer potential. For the first time, a scaling law was derived to predict the integral areal capacitance $C_{s,pred}$ of porous carbon electrodes as the product of an analytical expression (Eq. (16)) for the integral areal capacitance of a planar electrode $C_{s,planar}$ and a semi-empirical function $f(R_0^* - a^*/2)$ accounting for the porous electrode morphology. The latter was obtained using experimentally measured integral areal capacitance $C_{s,exp}$ for EDLCs with various porous carbon electrodes and binary electrolytes. The scaling law indicated that the integral areal capacitance was most sensitive to the ions' effective diameter and to the electrolyte dielectric constant. It was also sensitive to the pore radius R_0 only as R_0 approached the ion radius $a/2$. Overall, to achieve large integral areal capacitance (i) the effective ion diameter a should be small, (ii) the electrolyte dielectric constant ϵ_r should be large, (iii) the pore radius R_0 should be tailored to match the ion diameter, i.e., $2R_0 \approx a$, and (iv) the ion valency z should be large. The total energy stored can be further enhanced by increasing the surface potential ψ_s or the potential window and the interfacial area between electrode and electrolyte.

Acknowledgments

This material is based upon work supported as part of the Molecularly Engineered Energy Materials, an Energy Frontier Research Center funded by the U.S. Department of Energy, Office of Science, Office of Basic Energy Sciences under Award Number DE-SC0001342.

References

- [1] E. Frackowiak, Carbon materials for supercapacitor application, *Physical Chemistry Chemical Physics* 9 (15) (2007) 1774–1785.
- [2] P. Simon, Y. Gogotsi, Materials for electrochemical capacitors, *Nature Materials* 7 (11) (2008) 845–854.
- [3] L.L. Zhang, X.S. Zhao, Carbon-based materials as supercapacitor electrodes, *Chemical Society Reviews* 38 (9) (2009) 2520–2531.
- [4] D. Pech, M. Brunet, H. Durou, P. Huang, V. Mochalin, Y. Gogotsi, P.L. Taberna, P. Simon, Ultrahigh-power micrometre-sized supercapacitors based on onion-like carbon, *Nature Nanotechnology* 5 (9) (2010) 651–654.
- [5] A.J. Bard, L.R. Faulkner, *Electrochemical Methods: Fundamentals and Applications*, John Wiley & Sons, New York, NY, 2001.
- [6] J. Huang, B.G. Sumpter, V. Meunier, Theoretical model for nanoporous carbon supercapacitors, *Angewandte Chemie International Edition* 47 (3) (2008) 520–524.
- [7] J. Huang, B.G. Sumpter, V. Meunier, A universal model for nanoporous carbon supercapacitors applicable to diverse pore regimes, carbon materials, and electrolytes, *Chemistry – A European Journal* 14 (22) (2008) 6614–6626.
- [8] J. Huang, R. Qiao, B.G. Sumpter, V. Meunier, Effect of diffuse layer and pore shapes in mesoporous carbon supercapacitors, *Journal of Materials Research* 25 (8) (2010) 1469–1475.
- [9] J. Huang, B.G. Sumpter, V. Meunier, G. Yushin, C. Portet, Y. Gogotsi, Curvature effects in carbon nanomaterials: exohedral versus endohedral supercapacitors, *Journal of Materials Research* 25 (8) (2010) 1525–1531.
- [10] M.S. Kilic, M.Z. Bazant, A. Ajdari, Steric effects in the dynamics of electrolytes at large applied voltages. I. Double-layer charging, *Physical Review E* 75 (2) (2007), No. 021502.
- [11] M.S. Kilic, M.Z. Bazant, A. Ajdari, Steric effects in the dynamics of electrolytes at large applied voltages. II. Modified Poisson–Nernst–Planck equations, *Physical Review E* 75 (2) (2007), No. 021503.
- [12] E.M. Itskovich, A.A. Kornyshev, M.A. Vorotyntsev, Electric current across the metal–solid electrolyte interface I. Direct current, current–voltage characteristic, *Physica Status Solidi A* 39 (1) (1977) 229–238.
- [13] A.A. Kornyshev, M.A. Vorotyntsev, Conductivity and space charge phenomena in solid electrolytes with one mobile charge carrier species, a review with original material, *Electrochimica Acta* 26 (3) (1981) 303–323.
- [14] H. Wang, A. Thiele, L. Pilon, Simulations of cyclic voltammetry for electric double layers in asymmetric electrolytes: a generalized modified Poisson–Nernst–Planck model, *Journal of Physical Chemistry C* (2013) (in preparation).
- [15] M.Z. Bazant, M.S. Kilic, B.D. Storey, A. Ajdari, Towards an understanding of induced-charge electrokinetics at large applied voltages in concentrated solutions, *Advances in Colloid and Interface Science* 152 (1–2) (2009) 48–88.
- [16] H. Wang, L. Pilon, Accurate simulation of electric double layer capacitance for ultramicroelectrodes, *Journal of Physical Chemistry C* 115 (33) (2011) 16711–16719.
- [17] H. Wang, L. Pilon, Mesoscale modeling of electric double layer capacitors with three-dimensional ordered structures, *Journal of Power Sources* 221 (2013) 252–260.
- [18] J.H. Masliyah, S. Bhattacharjee, *Electrokinetic and Colloid Transport Phenomena*, John Wiley & Sons, Hoboken, NJ, 2006.
- [19] J. Lyklema, *Fundamentals of Interface and Colloid Science, Solid–Liquid Interfaces*, vol. II, Academic Press, San Diego, CA, 2001.
- [20] H. Wang, L. Pilon, Physical interpretation of cyclic voltammetry for measuring electric double layer capacitances, *Electrochimica Acta* 64 (2012) 130–139.
- [21] B.J. Kirby, *Micro- and Nanoscale Fluid Mechanics: Transport in Microfluidic Devices*, Cambridge University Press, New York, NY, 2010.
- [22] H. Wang, L. Pilon, Reply to commentary on intrinsic limitations of impedance measurements in determining electric double layer capacitances, *Electrochimica Acta* 76 (2012) 529–531.
- [23] J. Chmiola, G. Yushin, Y. Gogotsi, C. Portet, P. Simon, P.L. Taberna, Anomalous increase in carbon capacitance at pore sizes less than 1 nanometer, *Science* 313 (5794) (2006) 1760–1763.
- [24] H. Lu, W. Dai, M. Zheng, N. Li, G. Ji, J. Cao, Electrochemical capacitive behaviors of ordered mesoporous carbons with controllable pore sizes, *Journal of Power Sources* 209 (2012) 243–250.
- [25] K. Jurewicz, C. Vix-Guterl, E. Frackowiak, S. Saadallah, M. Reda, J. Parmentier, J. Patarin, F. Beguin, Capacitance properties of ordered porous carbon materials prepared by a templating procedure, *Journal of Physics and Chemistry of Solids* 65 (2/3) (2004) 287–293.
- [26] N. Liu, H. Song, X. Chen, Morphology control of ordered mesoporous carbons by changing HCl concentration, *Journal of Materials Chemistry* 21 (14) (2011) 5345–5351.
- [27] J. Wang, C. Xue, Y. Lv, F. Zhang, B. Tu, D. Zhao, Kilogram-scale synthesis of ordered mesoporous carbons and their electrochemical performance, *Carbon* 49 (13) (2011) 4580–4588.
- [28] H. Nishihara, H. Itoi, T. Kogure, P.X. Hou, H. Touhara, F. Okino, T. Kyotani, Investigation of the ion storage/transfer behavior in an electrical double-layer capacitor by using ordered microporous carbons as model materials, *Chemistry – A European Journal* 15 (21) (2009) 5355–5363.
- [29] D.S. Yuan, J. Zeng, J. Chen, Y. Liu, Highly ordered mesoporous carbon synthesized via in situ template for supercapacitors, *International Journal of Electrochemical Science* 4 (4) (2009) 562–570.
- [30] J. Yan, T. Wei, B. Shao, F. Ma, Z. Fan, M. Zhang, C. Zheng, Y. Shang, W. Qian, F. Wei, Electrochemical properties of graphene nanosheet/carbon black composites as electrodes for supercapacitors, *Carbon* 48 (6) (2010) 1731–1737.
- [31] D. Feng, Y. Lv, Z. Wu, Y. Dou, L. Han, Z. Sun, Y. Xia, G. Zheng, D. Zhao, Free-standing mesoporous carbon thin films with highly ordered pore architectures for nanodevices, *Journal of The American Chemical Society* 133 (38) (2011) 15148–15156.
- [32] J.-W. Lang, X.-B. Yan, X.-Y. Yuan, J. Yang, Q.-J. Xue, Study on the electrochemical properties of cubic ordered mesoporous carbon for supercapacitors, *Journal of Power Sources* 196 (23) (2011) 10472–10478.
- [33] Y. Lv, L. Gan, M. Liu, W. Xiong, Z. Xu, D. Zhu, D.S. Wright, A self-template synthesis of hierarchical porous carbon foams based on banana peel for supercapacitor electrodes, *Journal of Power Sources* 209 (2012) 152–157.
- [34] L. Jiang, J. Yan, L. Hao, R. Xue, G. Sun, B. Yi, High rate performance activated carbons prepared from ginkgo shells for electrochemical supercapacitors, *Carbon* 56 (2013) 146–154.
- [35] F. Li, M. Morris, K.-Y. Chan, Electrochemical capacitance and ionic transport in the mesoporous shell of a hierarchical porous core–shell carbon structure, *Journal of Materials Chemistry* 21 (24) (2011) 8880–8886.
- [36] J.N. Israelachvili, *Intermolecular and Surface Forces*, 3rd edition, Academic Press, San Diego, CA, 2010.
- [37] H. Wang, J. Varghese, L. Pilon, Simulation of electric double layer capacitors with mesoporous electrodes: effects of morphology and electrolyte permittivity, *Electrochimica Acta* 56 (17) (2011) 6189–6197.
- [38] J. Zhou, J. He, C. Zhang, T. Wang, D. Sun, Z. Di, D. Wang, Mesoporous carbon spheres with uniformly penetrating channels and their use as a supercapacitor electrode material, *Materials Characterization* 61 (1) (2010) 31–38.
- [39] F.B. Sillars, S.I. Fletcher, M. Mirzaei, P.J. Hall, Effect of activated carbon xerogel pore size on the capacitance performance of ionic liquid electrolytes, *Energy & Environmental Science* 4 (3) (2011) 695–706.
- [40] Y. Lv, F. Zhang, Y. Dou, Y. Zhai, J. Wang, H. Liu, Y. Xia, B. Tu, D. Zhao, A comprehensive study on KOH activation of ordered mesoporous carbons and their supercapacitor application, *Journal of Materials Chemistry* 22 (1) (2012) 93–99.